

# Two-electron one-photon process in collision of 1.8-2.1 MeV neon on aluminum

Shashank Singh,<sup>1</sup> Narendra Kumar,<sup>2</sup> Soumya Chatterjee,<sup>3</sup> Deepak Swami,<sup>4</sup>  
Alok Kumar Singh Jha,<sup>2</sup> Mumtaz Oswal,<sup>5</sup> K. P. Singh,<sup>1</sup> and T. Nandi<sup>6</sup>

<sup>1</sup>Department of Physics, Panjab University, Chandigarh-160014, India.

<sup>2</sup>School of physical sciences, JNU, New Delhi-110067, India

<sup>3</sup>Department of Physics, Brainware University, Barasat, Kolkata-700125, India

<sup>4</sup>Inter-University Accelerator Centre, Aruna Asaf Ali Marg, Near Vasant Kunj, New Delhi-110067, India.

<sup>5</sup>Department of Physics, DAV College, Sector 10, Chandigarh-160011, India.

<sup>6</sup>Department of Physics, Ramakrishna Mission Vivekananda Educational and Research Institute,  
PO Belur Math, Dist Howrah 711202, West Bengal, India\*

(Dated: January 7, 2025)

X-ray emissions due to the two-electron one-photon (TEOP) process in the neon projectile and aluminum target have been successfully observed for the beam energy window of 1.8-2.1 MeV. Experimental TEOP transition energies have been compared with theoretical predictions of flexible atomic structure code (FAC) and General-purpose Relativistic Atomic Structure (GRASP) package. Present results have been verified with reported theoretical and experimental values. Transition rates of the TEOP transitions have also been studied using the said codes. The observed lines have been assigned when the measured transition energies are in good agreement with the theoretical values. Such assignments have further been validated with the good agreements between the experimental and theoretical transition rates. Note that only the TEOP lines in projectile ions are seen with 1.8 MeV energy. In contrast, the TEOP lines in target ions are also observed well with 2.1 MeV energy. Thus, this study sheds useful light on the excitation mechanism of the TEOP processes in the low energy regimes.

In the heavy ion-atom collision processes, creation of multiple vacancies in different inner shells simultaneously is a common phenomenon. Sometimes the K shell of the target atom or projectile ions may be fully ionized. Normally two vacancies are filled in two steps, emission of hyper satellite and satellite x-ray lines are emitted one after another as pictorially shown in Fig. 1. Nevertheless, according to the prediction of [1-3], it is even possible that occasionally, both the vacancies of the K shell may be filled by a correlated jump of two electrons and only one photon is emitted. The energy of the two-electron one-photon (TEOP) transition ( $K^{-2} - L^{-2}$ ) can be estimated as the sum of the transition energies of hypersatellite ( $K^{-2} - K^{-1}L^{-1}$ ) and satellite transition ( $K^{-1}L^{-1} - L^{-2}$ ) energies. The schematic diagram of the TEOP transition is shown in the Fig. 1.

Wölflfi et al. [4] reported the TEOP transitions, for the

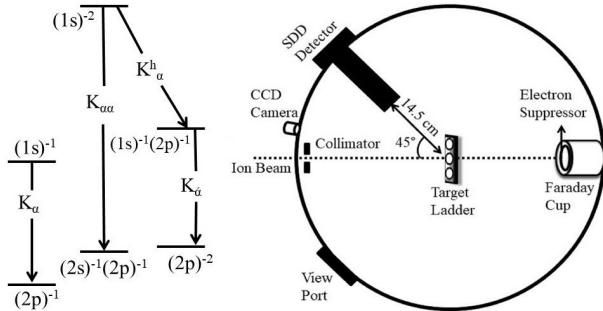


FIG. 1. Schematic of the two-electron one-photon transition (left) and experimental setup for the experiment (right).

first time, for Ni-Ni and Ni-Fe systems at beam energies  $\approx 0.8$  MeV/amu. Åberg et al.[5] showed that the TEOP transitions are due to the  $1s^{-2} \rightarrow 2s^{-1}2p^{-1}$  electric dipole transition by the calculations of the corresponding Hartree-Fock energy and transition probability. Various authors Wölflfi and Betz [6], Nagel et al. [7], Åberg et al. [5] and Knudson et al. [8] reported the theoretical prediction of TEOP transition energies in different systems to compare with the observed energies. In these works, Hartree-Fock energies have been consistent with the observed transition energies. Stoller et al. [9] measured the TEOP transitions for Al-Al, O-Ca, Ca-Ca, Fe-Fe, Fe-Ni, Ni-Fe and Ni-Ni systems at the beam energies between 24 to 40 MeV. In this study, cross-sections of characteristic transitions and TEOP transitions were determined. Also, branching ratios between one-electron one-photon (OEOP) and TEOP transitions in doubly ionized K shells were determined to compare with various theoretical predictions and found in qualitative agreement. Besides the ion-atom collisions, Auerhammer et al. [10] studied the TEOP transition in the aluminum target with electrons of energy 20 keV using a high resolution crystal spectrometer.

Mukherjee et al. [11] evaluated the branching ratio between OEOP and TEOP transitions in various atomic systems having doubly ionized K shell. Subsequently, Mukherjee and Mukherjee [12] reported the theoretical estimation of excitation energies and transition probabilities for TEOP transitions for the inner shell ionized atoms for He-like Ne, Na, Mg, Al, Si, P, S, Cl and Ar also. Both the OEOP and TEOP transitions in the atomic systems of fully vacant K-shell are very sensitive to Breit in-

teraction, quantum electrodynamics (QED), and electron correlations [13–15]. Experimental attempts have also been lodged to study such physics aspects by monochromatic synchrotron radiation on solid targets. Recently, Togawa et al. [16] observed the TEOP spectra by incident of photon on ions and compared transition energies well with the flexible atomic code (FAC) calculations [17].

The study of TEOP with the low energy heavy ions is very important for highly stripped ions of He- and Li-like ion sequences [18, 19] as such ions are present in solar corona, flares [20] and laboratory tokamak plasmas [21], but laboratory investigations on such systems are very sparse. We have intended to make a thorough experimental inspection on TEOP radiations using the low energy neon ions on aluminum target so that both the highly charged projectile and target ions can be used for the spectral analysis. We have obtained some intriguing results, which will be portrayed in detail.

This experiment was performed at the low energy ion beam facility, IUAC, New Delhi. In this experiment, we used  $\text{Ne}^{6+}$  beam of energies between 1.8 to 2.1 MeV. The ion beam was extracted from an electron cyclotron resonance ion source placed on a high voltage deck of 400 kV. The vacuum chamber was situated at the  $75^\circ$  beam line. The schematic of the scattering chamber with the experimental setup is shown in Fig. 1. A high vacuum around  $2 \times 10^{-6}$  Torr was maintained in the chamber. To detect the x-rays, one silicon drift detector (SDD) was mounted at  $135^\circ$  with respect to the beam direction. The specification of the SDD detector (KETEK AXAS-A) is as follows: active area =  $20 \text{ mm}^2$ , thickness of beryllium window =  $8 \mu\text{m}$  and full width at half maxima =  $124.2 \text{ eV}$  for Mn  $K_\alpha$  x-rays. The target ladder was mounted  $90^\circ$  with respect to the beam direction, which holds five targets at a time and a target was brought along the beam axis by a target manipulator. Spectroscopically pure aluminum targets were  $\approx 20 \mu\text{g}/\text{cm}^2$  measured by the energy loss of  $\alpha$ -beam from an  $^{241}\text{Am}$  source. The distance between the target ladder and detector was 14.5 cm. To measure the incident charge on the target, one Faraday cup was mounted behind the target and attached to a current integrator. A beam collimator of 5 mm diameter was placed at the entrance of the chamber.

Thickness of the mylar window for the SDD detector at the vacuum chamber used was  $10 \mu\text{m}$ . X-ray energy calibration was done before and after the experiment using an  $^{241}\text{Am}$  radioactive source. One position of the target of the target ladder was kept empty to study whether the beam hits the target frame or not. Furthermore, it also allowed us to compare the number of incident particles without the target and with the target in position using the Faraday cup. At another position of the target ladder a quartz crystal was placed to visualize the beam position. The online data were acquired using a CAMAC based software called FREEDOM [22].

The present calculations are performed using the

fully relativistic Multiconfiguration Dirac-Fock (MCDF) method [23] implemented in the General-purpose Relativistic Atomic Structure Package (GRASP) and the relativistic configuration interaction (RCI) technique imposed in flexible atomic code (FAC) [17]. An elaborate description of these two theories has been presented in Kumar et al. [24] and Flörs et al. [25], respectively. We have considered all the ionic states in both cases of neon and aluminum. To the best of knowledge such effort is hardly seen in literature. The details of it will be reported elsewhere. We have considered a number of configurations in every ionic state so that the results meet a convergence. It means both the transition energies and rates do not vary much either with additional configurations or with the length and velocity gauges. We skip to describe the methods here; however we must note that though the output of GRASP and FAC code comes in LS and JJ couplings respectively, we use the LS couplings only for our further use.

Studying x-ray spectroscopy of the light ions is very difficult, which can be understood from comparison of x-ray fluorescence yield as a function of atomic number [30, 31]. We can see from the data tables given in these articles that the value of the Auger transition rate is much higher than the x-ray emission rate for K shell transitions. The x-ray emission branch for neon and aluminum is only 1.89% and 5%, respectively. Furthermore, the large attenuation coefficient of low energy x-rays goes against having good statistics in the x-ray detections.

X-ray spectra recorded for  $\text{Ne}^{6+}$  beam on Al-target at 1.8 and 2.1 MeV have been shown in Fig. 2. Fig. 2(A) shows the raw spectra at 1.8 MeV containing a prominent Bremsstrahlung background and some weakly spectral lines overriding on this. Subtracting the background from the raw spectrum we obtain the net spectrum as shown in Fig. 2(B). The spectrum obtained shows a good peak structure in the region of 1.3 to 1.9 keV, which can be fitted into five Gaussian structures. Similar treatment was applied on the raw spectrum obtained with the 2.1 MeV  $\text{Ne}^{6+}$  beam also. Here, we see the similar structure in the region of 1.3-1.9 keV along with a structure around 3.0 keV.

The peak structure around 3.0 keV indicates its appearance due to the TEOP process in the aluminum target atoms, which can be fitted into two Gaussian peaks. To know the correct energy of these peaks, we calibrated the spectra further in a novel way. The bremsstrahlung backgrounds shown in both the spectra have two absorption dips as marked in the figure. They appear due to K-edge absorption of phosphorus [32] and chlorine [33] present as impurities in the aluminum target. Since the K absorption edges are very sharp and they are known within an eV uncertainties, internal calibration done with these dips refines further the earlier calibration with the radioactive x-ray sources mentioned above. With such a stringent calibration, the centroids of the neon and alu-

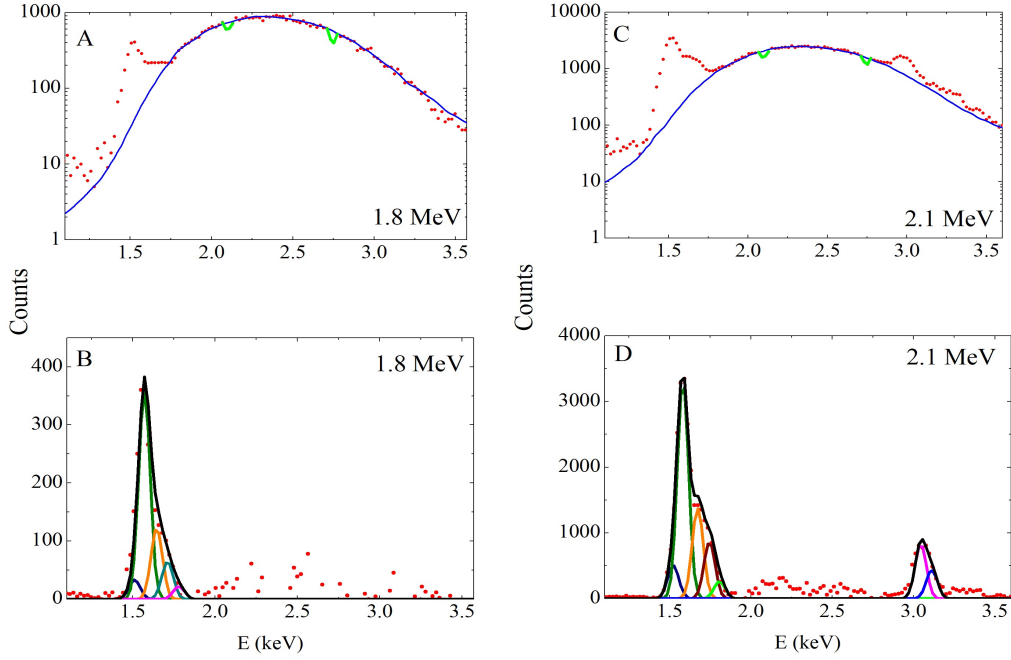


FIG. 2. (A and C) The Lines in blue represent the background spectra of the Ne ions on Al target at 1.8 and 2.1 MeV, respectively. (B and D) The background subtracted spectra are fitted with Gaussian peaks. The x-axis represents the x-ray energy in keV and y-axis the counts.

TABLE I. Testing the present calculation using the FAC and GRASP codes by comparing with the earlier theoretical as well as experimental results of transition energies (E) and rates (A). Two different transition energies shown with the same ref. [15] represent values with and without the higher order correlations.

El.	Trans.	Initial State	Final State	E(FAC)	E(GRASP)	Previous Results (E)		A(FAC)	A(GRASP)	Prev. Res. (A)
						Theory	Experiment			
Ne	$K_{\alpha\alpha}$	$1s^0 2s^2 2p^6 \ ^1S_0^e$	$1s^2 2s 2p^5 \ ^1P_1^o$	1.765	1.758	1.808 [12], 1.762 [26]		5.930E9	7.045E9	9.237E9 [12]
Ne	$K_{\alpha\alpha}$	$1s^0 2s^2 2p^5 \ ^2P_{3/2}^o$	$1s^2 2s 2p^4 \ ^2P_{3/2}^o$	1.789	1.793			4.014E9	3.509E9	
Ne	$K_{\alpha\alpha}$	$1s^0 2s^2 2p^4 \ ^1D_2^o$	$1s^2 2s 2p^3 \ ^1P_1^o$	1.797	1.804		1.8 [18]	8.098E9	9.280E9	
Ne	$K_{\alpha\alpha}$	$1s^0 2s^2 2p^3 \ ^2P_{3/2}^o$	$1s^2 2s^2 2p \ ^2P_{3/2}^e$	1.829	1.832			6.642E9	7.424E9	
Ne	$K_{\alpha\alpha}$	$1s^0 2s 2p \ ^1P_1^o$	$1s^2 \ ^1S_0^e$	1.927	1.926	1.924 [12]		1.066E9	3.004E9	4.514E9 [12]
Al	$K_{\alpha}$	$1s 2s^2 2p^6 3s^2 3p \ ^3P_0^o$	$1s^2 2s^2 2p^5 3s^2 3p \ ^3D_1^e$	1.487	1.492	1.486 [27]		1.258E13	1.546E13	
Al	$K_{\alpha}$	$1s 2s^2 2p^6 3s^2 \ ^2S_{1/2}^e$	$1s^2 2s^2 2p^5 3s^2 \ ^2P_{3/2}^o$	1.487	1.495			1.340E13	1.513E13	
Al	$K_{\alpha}$	$1s 2s^2 2p^6 \ ^2S_{1/2}^e$	$1s^2 2s^2 2p^5 \ ^2P_{3/2}^o$	1.489	1.493			1.479E13	1.557E13	
Al	$K_{\alpha}$	$1s 2s^2 2p^5 \ ^1P_1^o$	$1s^2 2s^2 2p^4 \ ^3P_2^e$	1.502	1.503			2.738E13	2.833E13	
Al	$K_{\alpha}$	$1s 2s^2 2p^4 \ ^4P_{5/2}^o$	$1s^2 2s^2 2p^3 \ ^2D_{5/2}^e$	1.514	1.513		$1.513 \pm 0.003$ [9] $1.497 \pm 0.011$ [10]	1.463E13	1.284E13	
Al	$K_{\alpha}^h$	$1s^0 2s^2 2p^6 3s^2 3p \ ^2P_{1/2}^o$	$1s^1 2s^2 2p^5 3s^2 3p \ ^2D_{3/2}^e$	1.613	1.619	1.627 [12], 1.622 [28]	$1.611 \pm 0.001$ [10]	2.995E13	3.552E13	1.547E13 [11]
Al	$K_{\alpha}^h$	$1s^0 2s^2 2p^6 3s^2 \ ^1S_0^e$	$1s^1 2s^2 2p^5 3s^2 \ ^1P_1^o$	1.614	1.621			5.187E13	6.188E13	
Al	$K_{\alpha}^h$	$1s^0 2s^2 2p^6 3s \ ^2S_{1/2}^e$	$1s^1 2s^2 2p^5 3s \ ^2P_{3/2}^o$	1.614	1.626			3.771E13	4.216E13	
Al	$K_{\alpha}^h$	$1s^0 2s^2 2p^6 \ ^1S_0^e$	$1s^1 2s^2 2p^5 \ ^1P_1^o$	1.615	1.627			6.144E13	6.548E13	1.275E13 [12]
Al	$K_{\alpha}^h$	$1s^0 2s^2 2p^5 \ ^2P_{3/2}^o$	$1s^1 2s^2 2p^4 \ ^4P_{3/2}^e$	1.627	1.634			2.446E13	2.566E13	
Al	$K_{\alpha}^h$	$1s^0 2s^2 2p^4 \ ^1S_0^e$	$1s^1 2s^2 2p^3 \ ^3S_1^o$	1.645	1.649		$1.648 \pm 0.001$ [9]	5.028E13	5.163E13	
Al	$K_{\alpha}^h$	$1s^0 2s^2 2p^3 \ ^4S_{3/2}^o$	$1s^1 2s^2 2p^2 \ ^4P_{3/2}^e$	1.661	1.662		$1.668 \pm 0.003$ [9]	2.054E13	2.037E13	
Al	$K_{\alpha}^h$	$1s^0 2s^2 2p^2 \ ^3P_0^o$	$1s^1 2s^2 2p \ ^3P_1^e$	1.680	1.683		$1.684 \pm 0.005$ [9]	3.082E13	3.019E13	
Al	$K_{\alpha}^h$	$1s^0 2s^2 2p^1 \ ^2P_{1/2}^o$	$1s^1 2s^2 \ ^2S_{1/2}^e$	1.695	1.694			1.582E13	1.723E13	
Al	$K_{\alpha\alpha}$	$1s^0 2s^2 2p^6 3s^2 3p \ ^2P_{1/2}^o$	$1s^2 2s 2p^5 3s^2 3p \ ^2D_{3/2}^e$	3.058	3.072	3.146 [11], 3.055 [15] 3.057 [28], 3.056 [29]	3.077 [11]	5.139E10	7.620E10	4.043E10 [11] 3.248E10 [15] 6.560E10 [29]
Al	$K_{\alpha\alpha}$	$1s^0 2s^2 2p^6 3s^2 \ ^1S_0^e$	$1s^2 2s 2p^5 3s^2 \ ^3S_0^e$	3.059	3.057	3.060 [15], 3.058 [15]		1.066E11	1.707E11	
Al	$K_{\alpha\alpha}$	$1s^0 2s^2 2p^6 3s \ ^2S_{1/2}^e$	$1s^2 2s 2p^5 3s \ ^2P_{1/2}^o$	3.060	3.089			1.478E10	1.353E10	
Al	$K_{\alpha\alpha}$	$1s^0 2s^2 2p^6 \ ^1S_0^e$	$1s^2 2s 2p^5 \ ^1P_1^o$	3.064	3.058			1.730E10	1.736E10	
Al	$K_{\alpha\alpha}$	$1s^0 2s^2 2p^5 \ ^2P_{3/2}^o$	$1s^2 2s 2p^4 \ ^2S_{1/2}^e$	3.094	3.103			9.259E9	8.218E9	1.628E10 [12]
Al	$K_{\alpha\alpha}$	$1s^0 2s^2 2p^4 \ ^1D_2^o$	$1s^2 2s 2p^3 \ ^1P_1^o$	3.121	3.127			1.758E10	2.022E10	
Al	$K_{\alpha\alpha}$	$1s^0 2s^2 2p^3 \ ^2S_{3/2}^o$	$1s^2 2s 2p^2 \ ^2P_{3/2}^e$	3.164	3.168			1.873E10	2.865E10	
Al	$K_{\alpha\alpha}$	$1s^0 2s^2 2p^2 \ ^4S_{3/2}^o$	$1s^2 2s 2p \ ^4P_{3/2}^e$	3.212	3.213			9.466E10	9.796E10	
Al	$K_{\alpha\alpha}$	$1s^0 2s^2 2p \ ^2P_{1/2}^o$	$1s^2 2s \ ^2S_{1/2}^e$	3.257	3.257			3.978E10	4.168E10	
Al	$K_{\alpha\alpha}$	$1s^0 2s 2p \ ^1P_1^o$	$1s^2 \ ^1S_0^e$	3.304	3.302	3.296 [12]		2.257E9	5.077E9	7.822E9 [12]

minimum x-ray lines are expected to be very correct.

Though the spectra shown in Fig. 2 do not show the neon K x-rays because of their absorption in the mylar window but the TEOP lines originated in neon projectile ions are observed at the right of the aluminum K x ray peaks. To know the spectroscopic origin of the neon as well as the aluminum TEOP lines we have made thorough calculations using the atomic structure codes GRASP and FAC as mentioned above. These calculations have been carried out as per the demand of the observed results in the present experiment, hence we have only considered the spectral lines having measurable emission rates of the order of  $10^9 \text{ s}^{-1}$  or more.

One important point is to mention here that in the present interaction, various ionic states can be possible not only with the projectile neon ions but also with the aluminum target atoms. Therefore, we have accounted for different charged states of both neon and aluminum ions. Charge state depended transition energies as well as rates have been calculated and listed in table I. Both the transition energies and rates have then been compared with both the available experimental and theoretical results. Comparison of present calculation with FAC code shows excellent agreement with the earlier theoretical calculations on both the transition energies and rates except those given in [11, 12]. This mismatch arises because the determination of screening parameters was tuned by hand instead of ab initio principles like other approaches including the present methods. Results obtained with the GRASP code are also reasonably good. Scenario of comparison of transition energies with earlier experimental values is also very good. Even the comparison of transition rates with earlier experimental figure is very good. For example, experimental intensity ratio  $I(K_{\alpha\alpha})/I(K_{\alpha}^h) = 2.2 \pm 0.8 \times 10^{-3}$  [10] agrees very well with that of FAC ( $1.72 \times 10^{-3}$ ) and GRASP ( $2.15 \times 10^{-3}$ ).

With the above mentioned success of our theoretical works, we decided to identify the observed spectral lines given in Table II with the help of our present calculations as listed in Table I. The spectral identifications so attributed give very good agreement except the lowest hypersatellite line in aluminum. The measured value  $1.576 \pm 0.012 \text{ keV}$  is quite lower than the FAC as well as GRASP predictions  $1.613 \text{ keV}$  and  $1.619 \text{ keV}$ , respectively. This line is the most intense, measurement uncertainty is thus the lowest. Still, this disagreement poses a surprise to us and thus, it is hard to know any reason for such difference at this stage.

Transition probabilities have been studied theoretically along with the transition energies so that predictive power of the theoretical calculations can be tested better by comparison with the measured values. Such a comparison has been displayed in Table III. Here, we have considered only the  $K_{\alpha\alpha}$  lines in the projectile as well as target ions because they are closed by and thus measurement uncertainty due to the quantum efficiency does not

differ considerably. The measured intensity ratio of  $K_{\alpha\alpha 1}$  to  $K_{\alpha\alpha 2}$  for neon and aluminum is about a factor of two and half, respectively in comparison to that of the theoretical ratios. It thus proves the good predictive power of both the theoretical procedures implemented in FAC and GRASP.

The present experiment was mainly planned to investigate the TEOP line in the target ions in the low energy regimes. Measurement was started with the 1.8 MeV neon beam, but no sign of the TEOP lines even after running the experiment for a long while. Then we took an attempt in performing the experiment with the highest available energy of 2.1 MeV and we noticed a mild signature of the TEOP lines in aluminum ions. Accordingly we continued the run for a long time to generate good statistics within the time allotted for the experiment. To check whether the first run was too short compared to the second run, we looked at the integrated charge counts in the Faraday cup. This quantity in the first run with 1.8 MeV energy was only a factor of 0.48 lower than that in the second run with 2.1 MeV energy. This fact is clearly reflected from the ratio of the bremsstrahlung peak observed at 1.8 MeV and 2.1 MeV energies. It thus suggests that the production rate of bremsstrahlung radiation with 1.8 and 2.1 MeV is almost the same.

As mentioned above, a remarkable feature observed in the present experiment is that 1.8 MeV Ne ion on Al target hardly show up any TEOP lines of Al whereas 2.1 MeV Ne ion impact shows clear signature of Al TEOP structure as seen in Fig. 2. This indicates that even a small increase of beam energy from 1.8 and 2.1 MeV changes the TEOP excitation in aluminum to a great extent. Reasons for such occurrences can be understood with comparison of the transition rates of  $K_{\alpha}^h$  and  $K_{\alpha\alpha}$ . The rates of the former are about three orders of magnitude higher than that of the latter. As a result though the  $K_{\alpha}^h$  lines are observed with 1.8 MeV Ne impacts, but no presence of  $K_{\alpha\alpha}$  structure is visible at all. We believe excitation function studies in this low energy regime will give us a significant idea of good impact energy that can populate the TEOP excitation well and conducting such experiments with high statistics will be possible. We believe in such a situation we can shed good light on the difference between the measured and calculated values on the line energy of the lowest  $K_{\alpha\alpha}$  line in Al. Furthermore, this study will help to understand the beam-foil mechanism also concerning the TEOP process. However, our accelerator facility does not provide with such scopes.

To conclude, we have succeeded to segregate the TEOP spectra from prominent Bremsstrahlung backgrounds in the interaction of slow Ne ions on Al target (90-95 keV/amu). The correct energy of the TEOP peaks are measured by incorporating the internal energy calibration by using the K absorption edges of the impurities of silicon and phosphorus present in the Al target. To assign such TEOP lines, we have made extensive calcula-

TABLE II. Measured line energies are listed and identified with the help of the present theoretical calculations as shown in Table I. Fifth column heading - ‘Expt.’ is the mean of two experimental readings at 1.8 MeV and 2.1 MeV.

El	Trans.	1.8 MeV	2.1 MeV	Expt.	Initial State	Final State	FAC	GRASP	A(FAC)	A(GRASP)
Al	$K_{\alpha}$	1.510±0.011	1.522±0.013	1.516±0.008	$1s^2s^22p^4 \ ^4P_{5/2}^e$	$1s^22s^22p^3 \ ^2D_{5/2}^o$	1.514	1.513	1.463E13	1.284E13
	$K_{\alpha}^h$	1.570±0.041	1.582±0.029	1.576±0.025	$1s^02s^22p^63s^23p \ ^2P_{1/2}^o$	$1s^12s^22p^53s^23p \ ^2D_{3/2}^e$	1.613	1.619	2.995E13	3.552E13
	$K_{\alpha}^h$	1.645±0.043	1.673±0.026	1.659±0.025	$1s^02s^22p^3 \ ^4S_{3/2}^o$	$1s^12s^22p^2 \ ^4P_{3/2}^e$	1.661	1.662	2.054E13	2.037E13
	$K_{\alpha\alpha 1}$	-	3.044±0.019	3.044±0.019	$1s^02s^22p^63s^23p \ ^2P_{1/2}^o$	$1s^22s^22p^53s^23p \ ^2D_{3/2}^e$	3.058	3.072	5.139E10	7.620E10
	$K_{\alpha\alpha 2}$	-	3.111±0.022	3.111±0.022	$1s^02s^22p^4 \ ^1D_2^o$	$1s^22s^22p^3 \ ^1P_1^o$	3.121	3.127	1.758E10	2.022E10
Ne	$K_{\alpha\alpha 1}$	1.710±0.037	1.745±0.026	1.728 ±0.022	$1s^02s^22p^6 \ ^1S_0^o$	$1s^22s^22p^5 \ ^1P_1^o$	1.765	1.758	5.930E9	7.045E9
	$K_{\alpha\alpha 2}$	1.779±0.018	1.807±0.020	1.793±0.013	$1s^02s^22p^5 \ ^2P_{3/2}^o$	$1s^22s^22p^4 \ ^2P_{3/2}^e$	1.789	1.793	4.014E9	3.509E9

TABLE III. Comparison of the measured line intensity ratios with the calculated ones in neon and aluminum ions.

El	Ratio	1.8 MeV	2.1 MeV	FAC	GRASP
Ne	$\frac{K_{\alpha\alpha 1}}{K_{\alpha\alpha 2}}$	2.90±0.4	3.26±0.3	1.48	2.01
Al	$\frac{K_{\alpha\alpha 1}}{K_{\alpha\alpha 2}}$		1.91±0.2	2.92	3.76

tions using the atomic structure codes GRASP and FAC. The calculations performed shows excellent agreement with the earlier experimental results. This assignment has further been verified with the comparison between measured and calculated transition rates. Another interesting observation is that 1.8 MeV Ne ion on Al target does not show up any TEOP lines of Al, whereas 2.1 MeV Ne ion impact on Al does. It means that even a small increase of beam energy from 1.8 and 2.1 MeV enhances the TEOP excitation in aluminum to a high level. Excitation function studies in this low energy regime will give us a significant idea to understand the beam-foil mechanism concerning the TEOP process.

The authors are thankful to the crew of LEIBF facility of IUAC consisting of Krishna Kant Pal, Amit Kumar and Pravin Kumar. They are also grateful to S.R. Abhilash and D. Kabiraj for providing necessary facility and support to making thin film targets. Further, Narendra Kumar expresses gratitude to Department of Science and Technology (DST) for awarding him Inspire—Senior Research Fellowship, award no. IF210224. Alok Kumar Singh Jha gratefully acknowledges the financial assistance provided by SERB, Department of Science and Technology (DST), Government of India under the research grant no. CRG/2022/008061.

\* Email: nanditapan@gmail.com (corresponding author)

- [1] Werner Heisenberg. Zur quantentheorie der multiplettstruktur und der anomalen zeemaneffekte. *Z. Phys.*, 32:841, 1925.
- [2] EU Condon. The theory of complex spectra. *Physical Review*, 36(7):1121, 1930.
- [3] S Goudsmit and L Gropper. Many-electron selection rules. *Physical Review*, 38(2):225, 1931.
- [4] W Wölfl, Ch Stoller, G Bonani, M Suter, and M Stöckli. Two-electron-one-photon transitions in heavy-ion collisions. *Physical Review Letters*, 35(10):656, 1975.
- [5] T Åberg, KA Jamison, and Patrick Richard. Origin of two-electron, one-photon k—x-ray transitions. *Physical Review Letters*, 37(1):63, 1976.
- [6] W Wölfl and Hans D Betz. Calculation of two-electron, one-photon k—x-ray transition energies. *Physical Review Letters*, 37(1):61, 1976.
- [7] DJ Nagel, PG Burkhalter, AR Knudson, and KW Hill. Two-electron, one-photon k x-ray transition energies. *Physical Review Letters*, 36(3):164, 1976.
- [8] AR Knudson, KW Hill, PG Burkhalter, and DJ Nagel. Energies and relative intensities of k  $\alpha\alpha$  x-ray transitions. *Physical Review Letters*, 37(11):679, 1976.
- [9] Ch Stoller, W Wölfl, G Bonani, M Stöckli, and M Suter. Two-electron one-photon transitions into the doubly ionized k shell. *Physical Review A*, 15(3):990, 1977.
- [10] J Auerhammer, H Genz, A Kumar, and A Richter. Two-electron-one-photon transition in aluminum following double-k-shell ionization. *Physical Review A*, 38(2):688, 1988.
- [11] Tapan Kumar Mukherjee, Jaideep Ghosh, and Sankar Sengupta. Branching ratio of two-electron-one-photon transitions in doubly ionized low-z atoms. *Physical Review A*, 42(5):3125, 1990.
- [12] TK Mukherjee and PK Mukherjee. Two electron one photon transitions in atomic systems. *Zeitschrift für Physik D Atoms, Molecules and Clusters*, 42(1):29–31, 1997.
- [13] R Diamant, S Huotari, Keijo Hämäläinen, CC Kao, and M Deutsch. Cu k h  $\alpha$  1, 2 hypersatellites: Suprathreshold evolution of a hollow-atom x-ray spectrum. *Physical Review A*, 62(5):052519, 2000.
- [14] JP Briand. Two-electron, one-photon transition energies. *Physical Review Letters*, 37(1):59, 1976.
- [15] Riddhi Kadrekar and L Natarajan. Two-electron one-photon transitions in atoms with  $12 \leq z \leq 80$ . *Journal of Physics B: Atomic, Molecular and Optical Physics*, 43(15):155001, 2010.
- [16] Moto Togawa, Steffen Kuhn, Chintan Shah, Pedro Amaro, Rene Steinbrugge, Jakob Stierhof, Natalie Hell, Marieke Rosner, Keisuke Fujii, Matthias Bissinger, et al. Observation of strong two-electron-one-photon transitions in few-electron ions. *Physical Review A*, 102(5):052831, 2020.
- [17] Ming Feng Gu. The flexible atomic code. *Canadian Journal of Physics*, 86(5):675–689, 2008.
- [18] S Andriamonje, HJ Andrä, and A Simionovici. Two electron-one photon x-ray emission in slow collisions between fully stripped ions and solids. *Zeitschrift für Physik D Atoms, Molecules and Clusters*, 21(1):S349–S350, 1991.

- [19] TK Mukherjee, TK Ghosh, and PK Mukherjee. On the interpretation of two electron-one photon transitions in slow collisions between fully stripped ions and solid target. *Zeitschrift für Physik D Atoms, Molecules and Clusters*, 33(1):7–9, 1995.
- [20] Takako Kato. Highly charged ions from solar flares. *Physica Scripta*, 1997(T73):98, 1997.
- [21] P Beiersdorfer. Highly charged ions in magnetic fusion plasmas: research opportunities and diagnostic necessities. *Journal of Physics B: Atomic, Molecular and Optical Physics*, 48(14):144017, 2015.
- [22] Data FREEDOM. Acquisition and analysis software, designed to support accelerator based experiments at the iuac.
- [23] IP Grant, BJ McKenzie, PH Norrington, DF Mayers, and NC Pyper. Atomic multiconfigurational dirac-fock package. *Comput. Phys. Commun.:(Netherlands)*, 21(2), 1980.
- [24] Narendra Kumar, Shivankar Shivankar, Alok Kumar Singh Jha, Mayank Dimri, Dishu Dawra, and Man Mohan. Relativistic atomic structure calculations, plasma and thermodynamic parameters for ca x. *The European Physical Journal Plus*, 138(12):1155, 2023.
- [25] Andreas Flörs, Ricardo F Silva, Jerome Deprince, Helena Carvajal Gallego, G Leck, LJ Shingles, Gabriel Martínez-Pinedo, JM Sampaio, P Amaro, JP Marques, et al. Opacities of singly and doubly ionized neodymium and uranium for kilonova emission modeling. *Monthly Notices of the Royal Astronomical Society*, 524(2):3083–3101, 2023.
- [26] M Gavrilă and JE Hansen. Calculation of  $k\alpha$ ,  $\alpha$  and  $kh\alpha$  transition rates. *Physics Letters A*, 58(3):158–160, 1976.
- [27] Herman Winick. X-ray data booklet. *X-RAY DATA BOOKLET*, 2009.
- [28] JK Saha, TK Mukherjee, S Fritzsche, and PK Mukherjee. The effect of a 2s vacancy on two-electron–one-photon lines: Relativistic approach. *Physics Letters A*, 373(2):252–255, 2009.
- [29] M. C. Martins, A. M. Costa, J. P. Santos, F. Parente, and P. Indelicato. Relativistic calculation of two-electron one-photon and hypersatellite transition energies for  $12 \leq z \leq 30$  elements. *Journal of Physics B: Atomic, Molecular and Optical Physics*, 37(19):3785, 2004.
- [30] Mau Hsiung Chen, Bernd Crasemann, and Hans Mark. Relativistic k-shell Auger rates, level widths, and fluorescence yields. *Physical Review A*, 21(2):436, 1980.
- [31] Mau Hsiung Chen. Auger transition rates and fluorescence yields for the double-k-hole state. *Physical Review A*, 44(1):239, 1991.
- [32] R Franke and J Hormes. The p k-near edge absorption spectra of phosphates. *Physica B: Condensed Matter*, 216(1-2):85–95, 1995.
- [33] Stosh A Kozimor, Ping Yang, Enrique R Batista, Kevin S Boland, Carol J Burns, David L Clark, Steven D Conradson, Richard L Martin, Marianne P Wilkerson, and Laura E Wolfsberg. Trends in covalency for d- and f-element metallocene dichlorides identified using chlorine k-edge x-ray absorption spectroscopy and time-dependent density functional theory. *Journal of the American Chemical Society*, 131(34):12125–12136, 2009.